Research Square

Preprints are preliminary reports that have not undergone peer review.
They should not be considered conclusive, used to inform clinical practice,
or referenced by the media as validated information.

Seasonal memory in Hudson Bay sea ice: autumn freeze-up predicts spring break-up, 1990–2026

Leo Wei

leocn0625@gmail.com

Beijing City International School https://orcid.org/0000-0003-2462-155X

Research Article

Keywords: Hudson Bay, sea ice, phenology, seasonal memory, freeze-up, break-up, machine learning, climate change

Posted Date: November 6th, 2026

DOI: https://doi.org/10.21203/rs.3.rs-11628631/v1

License: This work is licensed under a Creative Commons Attribution 4.0 International License.
Read Full License

Additional Declarations: The authors declare no competing interests.

Received: [for official use only] ; Accepted: [for official use only];
Managing Editor: [for official use only];
Action Editor: [for official use only]

Seasonal memory in Hudson Bay sea ice: autumn freeze-up predicts spring break-up, 1990–2026

Yuhan (Leo) Wei

Please note that this manuscript had been submitted for review at Convergence, A Journal for Young Researchers as of Nov. 2nd.

Abstract

Hudson Bay is one of the largest seasonally ice-covered seas in the Northern Hemisphere, and the timing of its ice season structures the regional climate, its marine ecosystems and the communities that depend on them. Between 1990 and 2026 the ice-free season lengthened by 6.8 days per decade. Most of that change is conventionally attributed to warming in the season in which it occurs, but here we show that the spring half of the signal cannot be explained that way: April–May air temperature over the bay has not risen, yet the date on which half the bay is open water has advanced by 2.8 days per decade. Using 37 ice seasons of daily 25-km satellite ice concentration, we develop a seasonal-memory model in which the preceding autumn's freeze-up date predicts the following spring's break-up independently of spring temperature. The relationship is strong (β = −0.50 days per day, $p < 0.001$, R^2 = 0.59) and survives first-differencing (β = −0.29, p = 0.025), instrumental-variable estimation (β = −0.58) and double machine learning (β = −0.40). The memory coefficient is negative in 89% of 1,428 grid cells and has grown from about −0.15 in 1990–2007 to −0.61 in 2008–2026, consistent with thinning ice. A two-predictor physical model outperforms gradient boosting with eleven predictors out of sample (R^2 = 0.48 versus 0.36), indicating that the relationship is additive and low-dimensional. Autumn freeze-up accounts for roughly 70% of the observed spring advance. Hudson Bay's ice-free season is therefore lengthening as a coupled two-season process, and autumn ice formation carries information about the following spring at a lead time of six months.

Keywords: Hudson Bay; sea ice; phenology; seasonal memory; freeze-up; break-up; machine learning; climate change

1. Introduction

Hudson Bay is a large, shallow, semi-enclosed sea on the southern margin of the North American Arctic. Together with James Bay it covers roughly 823,000 km² of marine area and drains a catchment of more than 3.5 million km², so that its surface is freshened by river discharge and its ice is seasonal rather than perennial. The bay freezes almost completely each winter and becomes largely ice-free each summer. That annual cycle governs the exchange of heat and moisture with the atmosphere, sets the timing and magnitude of primary

production, and provides the platform on which polar bears, ringed seals and other ice-dependent species depend (Derocher et al., 2004). The dates of freeze-up and break-up also define the travelling and hunting seasons for Inuit communities along the coast.

The bay sits at the southern edge of the cryosphere, where a small change in mean temperature can move the ice margin a long way. Global mean surface temperature rose by 0.23 K per decade between 1990 and 2025 in the NASA GISTEMP v4 record, and the 60–90°N mean rose by 0.66 K per decade over the same period, an amplification factor of 2.8. The decline is part of a wider Arctic signal: sea ice has retreated faster than early model projections (Stroeve et al., 2007), the melt season has lengthened (Markus et al., 2009; Stroeve et al., 2014), and the amplification itself is a documented feature of the Arctic system (Serreze & Barry, 2011). Hudson Bay warmed by 0.34 K per decade over 1990–2025, between the global and Arctic rates. It is therefore a natural place to look for the early expression of cryospheric change.

The response of the ice season has been documented before. Gagnon and Gough (2005) assembled weekly Canadian Ice Service charts for 36 locations over 1971–2003 and found significant trends toward earlier break-up in James Bay, along the southern shore and across the western half of the bay, and toward later freeze-up in the north. Hochheim and Barber (2010) showed that autumn ice-concentration anomalies over 1980–2005 were tightly coupled to surface air temperature and identified a regime shift in the mid-1990s. Later studies have extended the record and confirmed that the ice-free season is lengthening. These analyses share a common framing: each end of the ice season is treated as a response to atmospheric forcing in the same season, with break-up attributed to spring warmth and freeze-up to autumn cooling.

That framing leaves part of the signal unexplained. In the atmospheric reanalysis used here, April–May air temperature over the bay shows no detectable trend between 1990 and 2026 (Sen slope −0.28 K per decade, 95% confidence interval [−0.61, +0.13], $p = 0.14$). March and June are similarly flat. Yet the date on which half of the bay is open water has advanced by 2.8 days per decade ($p = 0.018$). Spring warmth alone cannot produce that advance, because spring warmth has not changed.

Sea ice, however, is a material with memory. Its thickness at the end of winter is the integral of the preceding autumn and winter, and a later freeze-up shortens the growth season. Stefan's law makes the dependence explicit: ice thickness grows approximately with the square root of accumulated freezing degree-days (Anderson, 1961). Seasonal forecasting studies exploit this memory, showing that Arctic sea-ice anomalies persist for months and provide skill at lead times of one to six months (Blanchard-Wrigglesworth et al., 2011; Day et al., 2014). If the same memory operates in Hudson Bay, the date of autumn freeze-up should carry information about the following spring's break-up, independently of how warm the spring turns out to be.

No study has quantified that coupling for Hudson Bay, tested whether it survives the obvious confounders, or asked whether it has changed as the ice has thinned. This paper does all three. We assemble 37 consecutive ice seasons of daily 25-km satellite ice concentration and daily atmospheric fields, define the ice season on

a September–August basis so that late freeze-ups are not censored, and formulate a seasonal-memory model in which break-up depends on the preceding freeze-up and on spring temperature.

We make four contributions. First, we show that the ice-free season lengthened by 6.8 days per decade over 1990–2026, that the autumn end contributed more than the spring end, and that the spring advance occurred without spring warming. Second, we estimate the autumn-to-spring coupling and subject it to three identification strategies: first-differencing, instrumental variables and double machine learning. Third, we estimate the model in every grid cell, which shows that the memory is a property of the bulk of the ice and is strongest where the ice season is shortest. Fourth, we benchmark the two-predictor model against gradient boosting and random forests, and we decompose the observed break-up trend into autumn and spring components.

The results reframe the lengthening of Hudson Bay's ice-free season. The spring retreat of the ice is not simply the local response to a warmer spring; it is substantially the delayed expression of the previous autumn. Section 2 describes the data and methods, Section 3 reports the results, and Section 4 discusses mechanism, implications and limitations.

2. Methods

2.1 Study region

The study domain is the marine area of Hudson Bay and James Bay. It is defined as the water body connected to a seed point at 57.5°N, 88°W in a 0.05° land–water mask derived from Natural Earth 1:10m coastlines, bounded at 63.5°N and 76°W so that Foxe Basin and Hudson Strait are excluded. The domain covers 823,087 km². On the 25-km passive-microwave grid used for the ice analysis, 1,428 cells have more than half of their area inside the domain and are retained.

2.2 Sea-ice observations

Daily sea-ice concentration was obtained from the National Snow and Ice Data Center Sea Ice Index, version 4.0 (G02135; Fetterer et al., 2017), on the 25-km polar-stereographic grid, for 1 September 1989 to 31 August 2026. The product merges SMMR, SSM/I and SSMIS passive-microwave retrievals and reports concentration as a percentage of each cell. Values above 100% (a retrieval artefact) were treated as missing. Bay-wide concentration was computed as the area-weighted mean of the cells, with cell areas corrected for the polar-stereographic scale factor. Daily fields were also retained on the native grid for the cell-level analysis.

2.3 The ice season and phenology

Calendar-year definitions right-censor freeze-up in years when the bay freezes late: in the 2024 season, 499 of the 1,428 cells had not reached 50% concentration by 31 December. We therefore define an ice season that

runs from 1 September to 31 August and is labelled by the calendar year of break-up. Within each ice season, freeze-up F is the first day on which bay-wide concentration reaches 50%, and break-up B is the first day after 1 March on which it falls below 50%. Days are counted from 1 September, so F is near day 98 (early December) and B near day 290 (mid-June). The ice-free season is $365 - (B - F)$. The 50% level is the date on which half of the bay is open water, a definition that is physically interpretable and insensitive to the behaviour of the last few percent of ice. Section 3.4 reports the sensitivity of the results to thresholds from 15% to 80%.

Per-cell dates were computed in the same way for every cell that retains at least half of its area inside the domain, giving a panel of 1,428 cells × 37 seasons. Because the ice season is defined continuously across the calendar year boundary, the panel has no missing seasons.

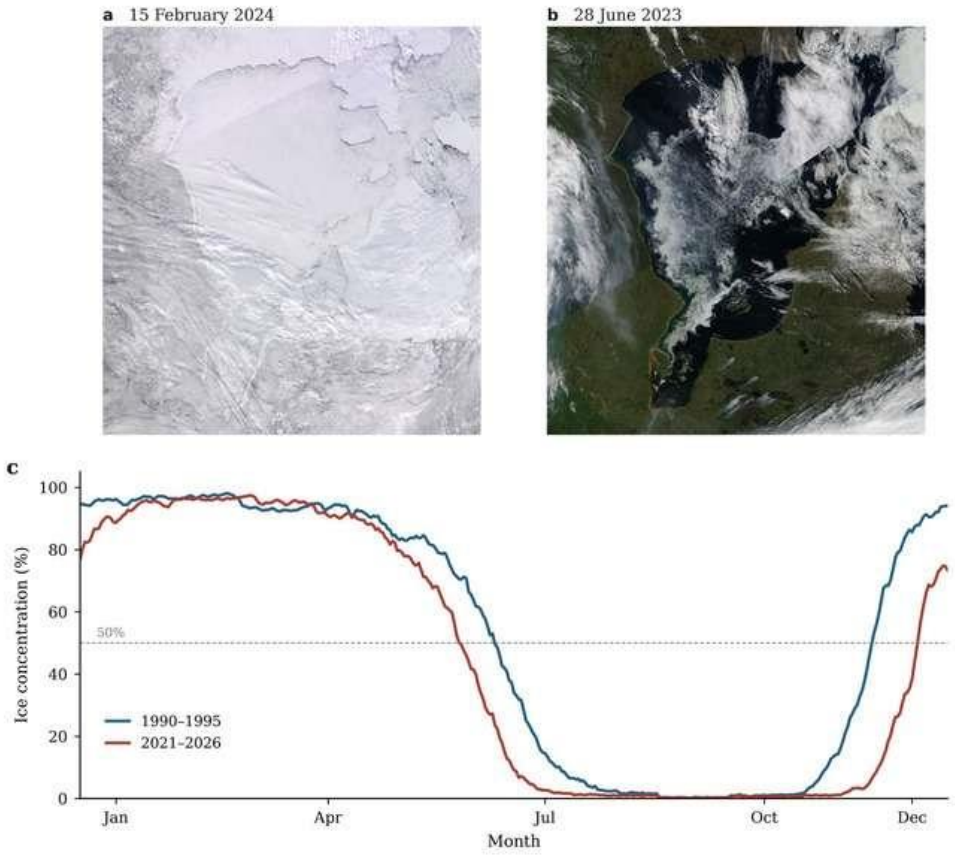


Figure 1. Hudson Bay in winter and in summer. (a) MODIS Terra corrected reflectance from NASA Worldview on 15 February 2024, when the bay is completely ice-covered. (b) The same layer on 28 June 2023, during break-up, with open water in the south and residual ice along the western and northern shores. (c) Mean daily ice concentration for 1990–1995 and 2021–2026. The later period freezes up later and breaks up earlier; the dashed line marks the 50% threshold used to define both dates.

2.4 Atmospheric and climate data

Daily meteorological fields were obtained from the NASA Prediction of Worldwide Energy Resources (POWER) service, which serves the MERRA-2 reanalysis (Gelaro et al., 2017). We used a 110-point grid covering the bay and a 300-km land ring at 1.5° latitude by 1.875° longitude spacing, for 1990–2026, with 19 variables including 2-m air temperature, surface skin temperature, downwelling shortwave and longwave radiation, 2-m wind speed, relative humidity, cloud amount, snow depth and precipitation (Table 1). Points were classified as bay or land ring using the domain mask and averaged area-weighted within each class. Spring temperature T is the mean April–May 2-m air temperature over the bay; autumn temperature is the mean September–November value for the autumn preceding each ice season.

Global and Arctic temperature anomalies were taken from NASA GISTEMP v4 (Lenssen et al., 2019) for context. Satellite imagery for Figure 1 was rendered from NASA Worldview, which serves GIBS imagery, using the MODIS Terra corrected-reflectance layer.

2.5 Trend estimation

Trends were estimated with the Sen–Theil slope (Sen, 1968) and tested with the Mann–Kendall statistic (Mann, 1945; Kendall, 1975), with the tie correction appropriate to a series of 37 annual values. The 95% confidence interval of the slope follows from the order statistics of the pairwise slopes. This combination makes no assumption of normality and is robust to the outlier years that characterize ice records.

2.6 The seasonal-memory model

For each ice season t we estimate

$$B_t = \alpha + \beta F_t + \gamma T_t + \varepsilon_t$$

where F is the freeze-up date of the same ice season, T is spring temperature, and ε is a residual. The coefficient β has units of days per day: it measures how many days earlier the bay breaks up for each day that it froze later. The two predictors are almost uncorrelated in the sample ($r = 0.04$), so their coefficients are separately identified by the data rather than by prior assumptions. Standard errors are conventional least-squares standard errors; all inferences were checked by bootstrap.

2.7 Identification

A correlation between two trending seasonal dates can arise from a shared trend rather than from a causal link. We therefore subject the model to three further specifications.

First differences. Regressing year-to-year changes in break-up on year-to-year changes in freeze-up and spring temperature removes any common linear trend and any time-invariant confounder. A negative

coefficient in differences means that a year in which the bay froze later than the previous year tended to break up earlier than the previous year.

Instrumental variables. Autumn temperature is a strong predictor of freeze-up (first-stage $F = 109$) and is plausibly unrelated to spring break-up except through the state of the ice. We use September–November air temperature as an instrument for F in a two-stage least-squares model, controlling for spring temperature, and report heteroskedasticity-robust standard errors. The exclusion restriction would fail if autumn warmth affected spring break-up through ocean heat storage rather than through the ice; we regard that channel as part of the same seasonal-memory pathway, but we flag it as an assumption rather than a result.

Double machine learning. We also estimate β by partialling out a flexible, cross-fitted gradient-boosting model of nine atmospheric covariates (spring and winter temperature, wind, cloud, downwelling longwave and shortwave radiation, snow depth, the previous year's break-up date and the previous season's length), following the double/debiased machine-learning framework of Chernozhukov et al. (2018). This allows the nuisance relationship between the covariates and both break-up and freeze-up to be nonlinear, while the memory parameter is estimated linearly.

2.8 Spatial estimation

The memory model was estimated separately in each of the 1,428 cells, with bay-wide spring temperature as the control. This yields a map of β and a distribution that can be compared with the spatial pattern of ice-season length. Because neighbouring cells are not independent, inference at the cell level is descriptive; the basin-scale estimate carries the formal inference.

2.9 Machine-learning benchmark

To ask whether the relationship is more complex than a two-term linear model, we compared four models on identical leave-one-year-out cross-validation: the two-predictor memory model; a linear model with eleven predictors; gradient boosting with shallow trees (Friedman, 2001); and a random forest (Breiman, 2001). The eleven predictors are freeze-up date, spring temperature, winter temperature, autumn temperature, spring wind, spring cloud, spring downwelling longwave and shortwave radiation, maximum snow depth, the previous year's break-up date and the previous season's length. All are available before break-up. Out-of-sample R^2 and root-mean-square error were computed from the held-out predictions. Driver importance was assessed with TreeSHAP (Lundberg & Lee, 2017) on a gradient-boosting model fitted to the full sample.

2.10 Software and reproducibility

Analyses were carried out in Python 3.12 with NumPy, pandas, SciPy, statsmodels, scikit-learn, SHAP, xarray, rasterio, cartopy and linearmodels. All data sources are public. The processing and analysis code, together with the derived annual and cell-level tables, is provided as Appendix A and in the accompanying repository.

Table 1

Data sources.

Dataset	Variables used	Resolution	Period	Provider
Sea Ice Index G02135 v4.0	Daily sea-ice concentration	25 km; daily	Sep 1989–Aug 2026	NSIDC
MERRA-2 via NASA POWER	2-m and skin temperature, radiation, wind, humidity, cloud, snow, precipitation (19 variables)	1.5°×1.875° grid; daily	1990–2026	NASA GMAO / LaRC
GISTEMP v4	Global and 60–90°N temperature anomalies	2°×2°; monthly	1990–2025	NASA GISS
Worldview / GIBS	MODIS Terra corrected reflectance	250 m	scene date	NASA EOSDIS

Note. All products are publicly available without registration. The atmospheric grid comprises 110 points: those inside the bay domain and those within 300 km of it on land.

3. Results

3.1 The ice-free season lengthens at both ends

Over the 37 ice seasons from 1990 to 2026, Hudson Bay broke up on average on day 290 (17 June) and froze on average on day 98 (7 December), giving a mean ice-free season of 173 days. Both ends moved (Figure 2; Table 2). Break-up advanced by 2.8 days per decade (95% CI [−5.3, −0.5], p = 0.018) and freeze-up retreated by 4.0 days per decade ([+1.4, +6.1], p = 0.003). The ice-free season therefore lengthened by 6.8 days per decade ([+3.2, +11.0], p = 0.004).

The change is large in absolute terms. The seven seasons from 1990 to 1996 averaged a 156-day ice-free season; the seven from 2020 to 2026 averaged 186 days. In the early period half the bay was open by about 25 June and half was frozen by about 28 November; in the late period the corresponding dates were about 11 June and 14 December.

Freeze-up carries the larger share of the change, both in slope and in statistical strength. Its trend is more than twice as well determined as the break-up trend (p = 0.003 against p = 0.018), and it is robust across every concentration threshold we tested, from 15% to 80% (+4.0 to +4.6 days per decade in all cases). Break-up is more variable from year to year: the earliest season in the record (2024, day 275) and the latest (1992, day 311) are 36 days apart, and a single anomalous spring can move the fitted trend appreciably.

Table 2

Trends in ice-season dates and seasonal air temperature, 1990–2026.

Quantity	Mean	Sen slope	95% CI	p
Break-up date (day of ice season)	290.0 (17 Jun)	−2.81 d dec^{-1}	[−5.26, −0.45]	0.018
Freeze-up date (day of ice season)	98.4 (7 Dec)	+4.00 d dec^{-1}	[+1.43, +6.11]	0.003
Ice-free season length	173.4 d	+6.84 d dec^{-1}	[+3.20, +11.00]	0.004
Spring temperature, Apr–May	−6.54 °C	−0.28 K dec^{-1}	[−0.61, +0.13]	0.14
Autumn temperature, Sep–Nov	+0.85 °C	+0.71 K dec^{-1}	[+0.31, +1.09]	0.002
Winter temperature, Jan–Mar	−20.17 °C	−0.08 K dec^{-1}	[−0.58, +0.41]	0.85
Annual bay temperature	+0.34 K (anom.)	+0.34 K dec^{-1}	[+0.06, +0.62]	0.027

Note. Sen–Theil slopes with Mann–Kendall tests, n = 37 ice seasons (1990–2026) for ice dates and 36 years (1990–2025) for temperature. Day of ice season counts from 1 September. Confidence intervals are the 95% order-statistic intervals of the pairwise slopes.

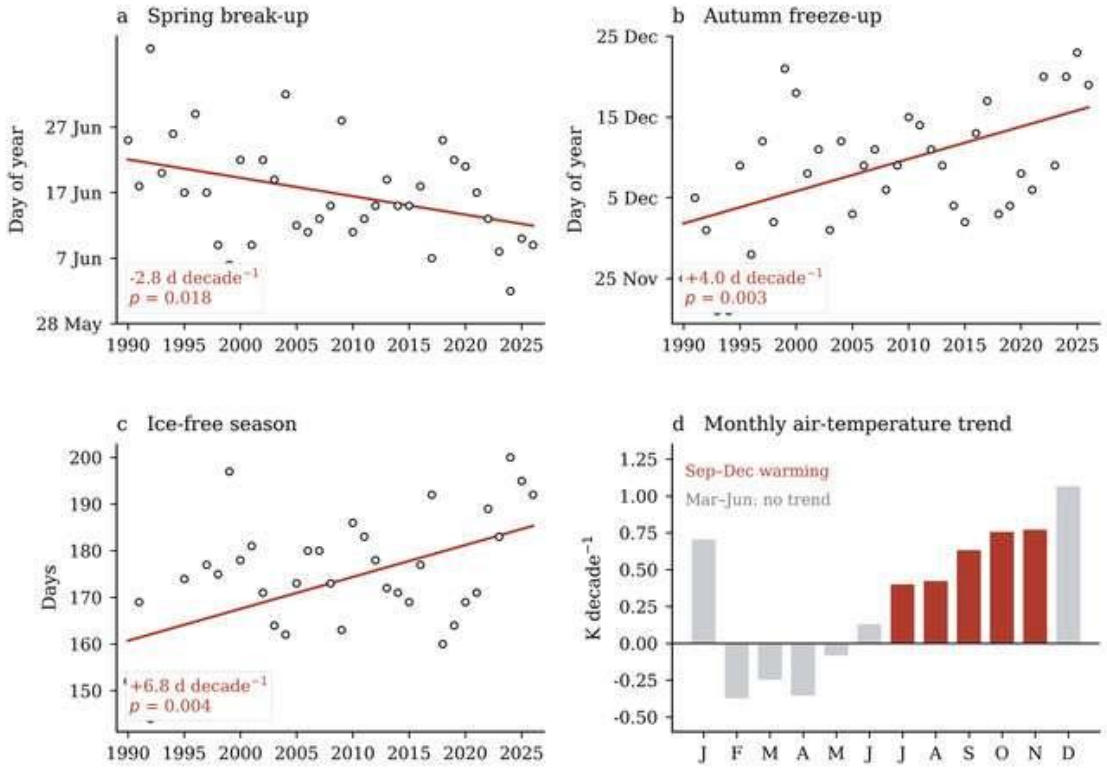


Figure 2. Observed changes in the ice season and in atmospheric forcing. (a) Break-up date, (b) freeze-up date and (c) ice-free season length, 1990–2026, with Sen–Theil fits. (d) Sen trends in bay-mean 2-m air temperature by calendar month, 1990–2025; red bars mark $p < 0.05$ and grey bars $p \geq 0.05$. The spring months in which the ice disappears show no significant warming, whereas September–December warm strongly.

3.2 *Spring has not warmed*

Figure 2d shows the trend in bay-mean air temperature for each calendar month over 1990–2025. The warming is strongly seasonal. September, October and November warm by 0.6–0.8 K per decade ($p < 0.05$ in each month), and December by 0.9 K per decade ($p = 0.03$). July and August warm by about 0.4 K per decade. From March to June, by contrast, no month shows a significant trend, and the point estimates for March, April and May are negative (−0.17, −0.22 and +0.02 K per decade respectively).

The spring season as a whole, April–May, has a Sen slope of −0.28 K per decade (95% CI [−0.61, +0.13], $p = 0.14$). Winter, January–March, is flat (−0.08 K per decade, $p = 0.85$). Autumn, September–November of the preceding year, warms by 0.71 K per decade ($p = 0.002$).

This asymmetry is the central empirical fact of the paper. The season in which the ice disappears has not warmed, while the season in which it forms has warmed substantially. A model in which break-up responds only to spring temperature cannot reproduce the observed advance of break-up.

3.3 *Autumn freeze-up predicts spring break-up*

The seasonal-memory model resolves the puzzle. Regressing break-up date on freeze-up date and spring temperature gives

$$B = 316.4 - 0.496\,F - 3.433\,T, \quad R^2 = 0.585$$

with both coefficients significant at $p < 0.001$. The freeze-up coefficient implies that a bay that freezes ten days later in autumn breaks up about five days earlier the following spring, holding spring temperature fixed. In standardized units the two predictors are almost equally important ($\beta = -0.50$ for freeze-up and −0.56 for spring temperature), despite freeze-up receiving no attention in conventional spring-forcing accounts. The model explains 59% of the variance in break-up date, against 27% for freeze-up alone and 33% for spring temperature alone.

Figure 3a shows the relationship as a partial-residual plot: the vertical axis is the component of break-up not explained by spring temperature, and the horizontal axis is the component of freeze-up not explained by spring temperature. The negative slope is not an artefact of the shared trend, because both axes have had the spring-temperature signal removed.

3.4 *Test of The relationship on differencing, instrumentation and flexible adjustment*

Three further specifications are reported in Table 3. In first differences, the coefficient is −0.29 (standard error 0.12, $p = 0.025$) with spring temperature controlled, and the model explains 65% of the variance in year-to-year changes. The instrumental-variable estimate, using autumn temperature as an instrument for freeze-up, is −0.58 (95% CI [−0.82, −0.33], $p < 0.001$); the first stage has an F statistic of 109, so weak

instruments are not a concern. The double machine-learning estimate, which partials out nine atmospheric covariates flexibly, is −0.40 (95% CI [−0.68, −0.12]).

The IV estimate is larger in magnitude than the least-squares estimate, which is what one expects when the regressor is measured with noise: classical attenuation biases the least-squares coefficient toward zero. The double-machine-learning estimate lies between the two. All three strategies agree on the sign, the order of magnitude and the statistical significance of the memory term.

Table 3

The seasonal-memory coefficient under alternative identification strategies.

Specification	β (d d⁻¹)	95% CI	p	R^2	n
Levels, OLS	−0.496	[−0.71, −0.28]	<0.001	0.585	37
First differences	−0.286	[−0.53, −0.04]	0.025	0.648	36
Instrumental variables (2SLS)	−0.575	[−0.82, −0.33]	<0.001	—	37
Double machine learning	−0.402	[−0.68, −0.12]	0.004	—	37
Double ML with autumn temperature	−0.115	[−0.53, +0.30]	0.60	—	37
1990–2007 subsample	−0.152	[−0.41, +0.11]	0.23	—	18
2008–2026 subsample	−0.613	[−0.85, −0.37]	<0.001	—	19

Note. Every specification controls for April–May bay-mean air temperature. β is in days of break-up date per day of freeze-up date. In the instrumental-variable model, September–November air temperature instruments for freeze-up; the first-stage *F* statistic is 109. The double-machine-learning model partials out nine atmospheric covariates with cross-fitted gradient boosting. The final two rows split the record at 2007 to show the change in the coefficient over time.

One caveat applies to the double-machine-learning specification. When autumn temperature is added to the covariate set, the memory coefficient collapses to −0.12 (95% CI [−0.53, +0.30]). This is not evidence against the memory: autumn temperature and freeze-up date are almost collinear (r = 0.88), and the two variables compete for the same variance. The collapse indicates that the model cannot separate the effect of autumn warmth from the effect of the freeze-up date it produces, which is the expected behaviour of a causal chain in which one variable mediates the other.

Table 4

Robustness of the memory coefficient to the concentration threshold.

Threshold (%)	β (d d⁻¹)	p	Freeze-up trend (d dec⁻¹)	Break-up trend (d dec⁻¹)
15	−0.59	<0.001	+4.1	−2.4
25	−0.54	<0.001	+4.0	−2.6
35	−0.51	<0.001	+4.0	−2.7
50 (primary)	−0.50	<0.001	+4.0	−2.8
60	−0.43	0.002	+4.2	−3.1
70	−0.27	0.041	+4.6	−3.4
80	−0.05	0.71	+4.5	−3.6

Note. The memory model was re-estimated with freeze-up and break-up defined at each threshold. The relationship is stable from 15% to 70% and vanishes at 80%, where the residual ice is controlled by local winds rather than by the integrated growth season.

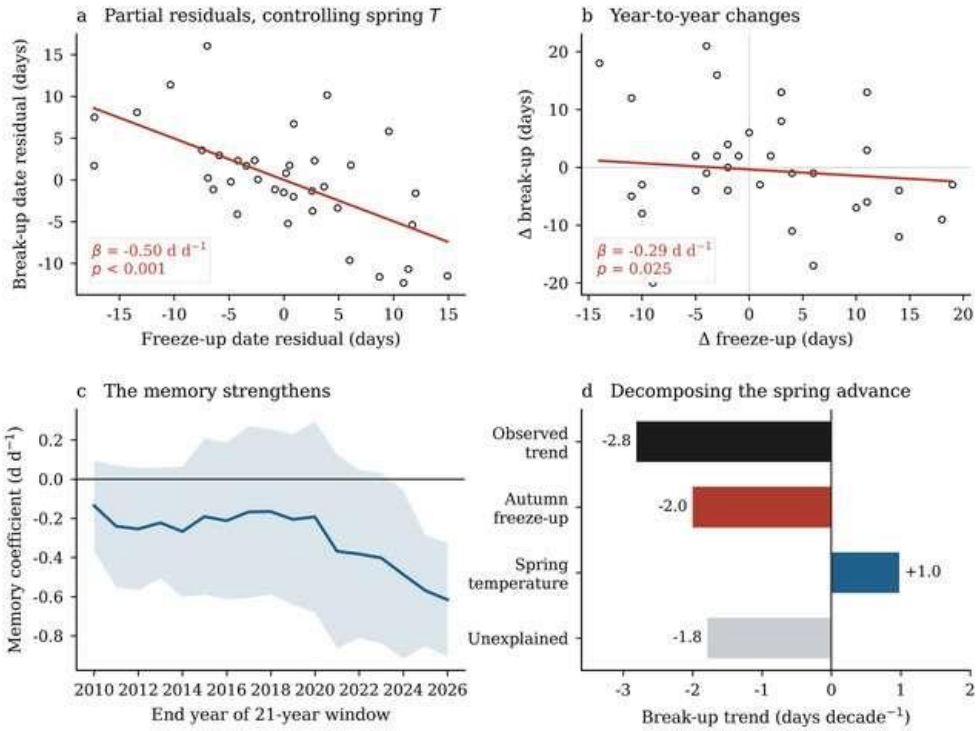


Figure 3. Seasonal memory. (a) Partial-residual plot of break-up against freeze-up after removing the spring-temperature signal; the line is the fitted memory coefficient. (b) Year-to-year changes in break-up against year-to-year changes in freeze-up; the first-difference estimate removes any common trend. (c) The memory coefficient in rolling 21-season windows, with the 95% confidence band. (d) Decomposition of the observed break-up trend into an autumn term, a spring term and a residual.

3.5 *The memory has strengthened*

Allowing the memory coefficient to change linearly with time gives an interaction of −0.14 days per day per decade ($p = 0.063$). Splitting the record at 2007 makes the change easier to read. In 1990–2007 the coefficient is −0.15 ($p = 0.23$, $n = 18$); in 2008–2026 it is −0.61 ($p < 0.001$, $n = 19$). The difference between the two eras, −0.46 days per day, is stable to leave-one-year-out resampling (range −0.37 to −0.52).

Rolling 21-year windows tell the same story more gradually (Figure 3c). The coefficient is about −0.14 for the window ending in 2010, remains between −0.15 and −0.27 through the 2010s, and falls to −0.62 by 2026. The strengthening is not monotonic, and the interaction term on its own is only marginally significant; we therefore treat the trend in the coefficient as suggestive rather than established.

A nonlinear alternative deserves consideration. If the relationship between freeze-up and break-up is convex, then a shift toward later freeze-ups would move the system along a steeper part of a fixed curve and produce an apparent strengthening without any change in the underlying physics. A quadratic term in freeze-up is not significant ($p = 0.37$), and adding it leaves the interaction substantially unchanged, but 37 seasons provide limited power to distinguish the two explanations. Both are consistent with thinning ice, and the distinction does not affect the main result.

3.6 *Spatial structure*

Estimating the model cell by cell shows that the memory is a property of the ice as a whole rather than of a few locations (Figure 4). The median coefficient across 1,428 cells is −0.34 days per day, with an interquartile range of −0.55 to −0.15. It is negative in 89% of cells and individually significant at the 5% level in 30%. Positive coefficients occur mainly along the northern and eastern margins, where the local ice season is short and the 50% threshold is reached close to the limits of the retrieval.

The spatial pattern is informative. Cells with a shorter mean ice-covered season have more negative memory coefficients ($r = +0.26$, $p < 0.001$ between the coefficient and the mean ice-covered season), which is the signature of a thickness effect: where ice has less time to grow, its spring fate is more sensitive to when growth began. The memory coefficient is also correlated with the local break-up trend ($r = +0.53$), so the places where the memory is strongest are the places where break-up has advanced most.

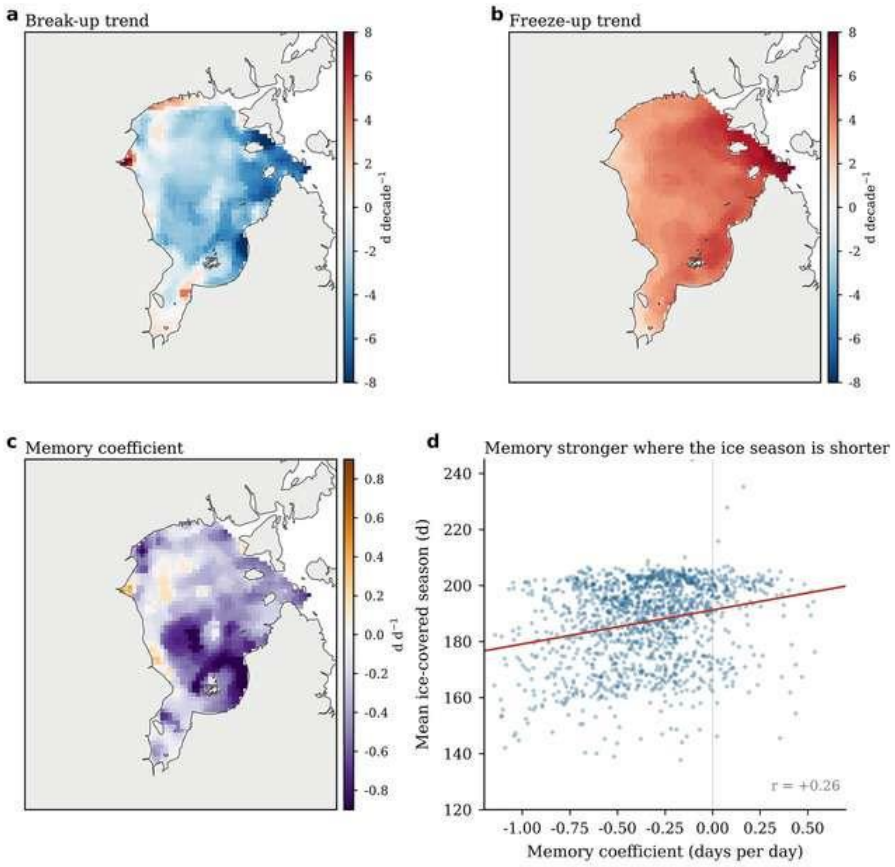


Figure 4. Spatial structure. (a) Local Sen trend in break-up date and (b) in freeze-up date, in days per decade. (c) The memory coefficient estimated separately in each of 1,428 cells. (d) Memory coefficient against the mean length of the ice-covered season in the same cell: the memory is stronger where the ice season is shorter.

3.7 A *simple model outperforms machine learning*

Leave-one-year-out cross-validation shows that the two-predictor model is the best of the four models tested (Figure 5). Its out-of-sample R^2 is 0.48 with a root-mean-square error of 5.6 days, against 0.27 for a linear model with eleven predictors, 0.36 for gradient boosting and 0.34 for a random forest. Adding nine predictors therefore degrades prediction, because 37 observations cannot support the additional degrees of freedom.

The machine-learning models are nevertheless useful as a check on functional form. TreeSHAP attribution on the gradient-boosting model ranks spring temperature first (2.5 days), autumn temperature second (1.9 days), spring cloud third (1.3 days) and freeze-up fourth (1.2 days). Autumn variables therefore occupy two of the top four positions, even though the model was given eleven candidates. The failure of the flexible models

to improve on the linear model indicates that the relationship is additive and close to linear over the observed range, which is what the physical account predicts.

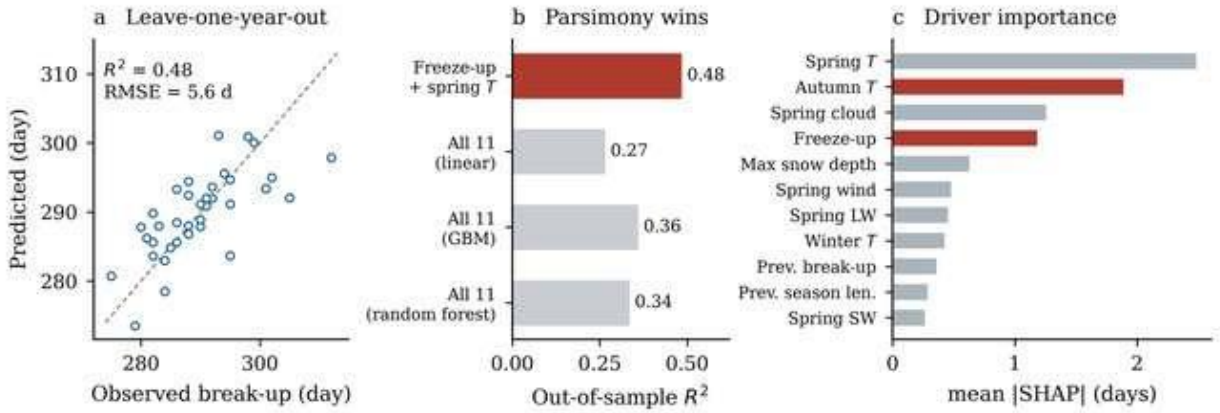


Figure 5. Machine-learning benchmark and driver importance. (a) Observed and predicted break-up dates under leave-one-year-out cross-validation for the two-predictor memory model. (b) Out-of-sample R^2 for that model, an eleven-predictor linear model, gradient boosting and a random forest. (c) Mean absolute TreeSHAP attributions from the gradient-boosting model, in days of break-up date; autumn variables occupy two of the four leading positions.

3.8 Decomposition of the break-up trend

Combining the fitted model with the observed trends allows the break-up advance to be decomposed (Figure 3d). The observed trend is −2.8 days per decade. Multiplying the freeze-up coefficient by the freeze-up trend gives −2.0 days per decade, or about 71% of the observed change. Spring temperature contributes +1.0 day per decade, because its point estimate is slightly negative and a cooler spring would delay break-up; this term offsets part of the autumn effect. The remaining −1.8 days per decade is not captured by the two predictors and reflects either nonlinearity, changes in other drivers, or the imperfect observation of both dates.

The decomposition should be read as an accounting exercise instead of as a structural attribution. It says that the autumn term is large enough to account for most of the observed spring advance, not that the residual has been explained.

4. Discussion

4.1 Mechanism

The most parsimonious mechanism is thickness. Sea ice grows by conducting heat from the ocean to the cold atmosphere, and its thickness increases approximately with the square root of accumulated freezing degree-days. A freeze-up that occurs two weeks later leaves two weeks less time for growth, and the ice that

forms is thinner at the start of spring. Thinner ice requires less energy to melt through, so break-up arrives earlier for the same spring forcing.

Two features of the data support this account. First, the memory coefficient strengthens as the ice-covered season shortens, both across space (Section 3.6) and through time (Section 3.5). If the coupling were a fixed atmospheric teleconnection, there is no obvious reason for it to depend on the length of the ice season. Second, the relationship is strongest for the bulk of the ice and weakens at the 70% threshold before disappearing at 80% (Table 4). The last fifth of the ice is controlled by local winds and by the residual thickness of the thickest floes, not by the integrated growth season.

We cannot test the thickness mechanism directly, because no basin-wide thickness product covers Hudson Bay for the full period. The inference is therefore indirect. Satellite altimetry from ICESat-2 and CryoSat-2 now provides winter thickness estimates for the bay, and combining those with the present framework is the obvious next step.

4.2 Why the autumn end dominates

Autumn is where the warming is. September–November air temperature over the bay has risen by 0.71 K per decade since 1990, while April–May has not risen at all. The autumn signal is amplified by an ice–albedo feedback that operates in the dark season through ocean heat storage: later freeze-up leaves open water exposed for longer, the ocean absorbs more heat during the low-sun period, and the extra heat further delays freeze-up. The same feedback is weak in spring, when the ice is still present and surface albedo remains high until the ice has gone.

This asymmetry explains a pattern that has puzzled previous analyses of the region: why break-up advances at all when spring temperatures are flat. It also predicts that the autumn end should continue to lead the spring end as warming proceeds, at least until the ice becomes so thin that spring conditions dominate completely.

4.3 Implications

The practical consequence is predictability. If the autumn freeze-up date carries a coefficient of −0.5 days per day into the following spring, then an observation made in December constrains the break-up date six months later. The out-of-sample skill of the two-predictor model, $R^2 = 0.48$ with an error of 5.6 days, is comparable to that of dynamical seasonal forecasts for the region and is obtained from two numbers. For communities that depend on the ice for travel, for shipping operators planning the sealift season, and for wildlife managers monitoring body condition of polar bears, a six-month lead time is operationally useful.

For ecology, the result changes the interpretation of the ice-free season. A longer ice-free season is not simply more open water in summer; it is also a shorter growth season in winter, which is the period during

which the ice accumulates the thickness on which spring persistence depends. The two effects are coupled, and treating them separately will misstate the rate at which the bay is changing.

4.4 *Limitations*

Several limitations qualify these findings. First, the analysis is observational. The three identification strategies address trend confounding, measurement error and flexible adjustment, but none of them rules out an unobserved seasonal atmospheric mode that makes both autumn and spring anomalous in the same direction. The first-difference and instrumental-variable results make that explanation less likely, but they do not eliminate it.

Second, the record is 37 seasons long. That is enough to detect the memory coefficient with confidence, but only marginally enough to establish that the coefficient has changed over time. We report the strengthening as suggestive and give the interaction p value explicitly.

Third, the forcing is taken from a reanalysis whose spatial resolution (1.5° by 1.875°) is coarse relative to the ice grid, and which assimilates few observations over the bay itself. Gridded reanalyses in the region are known to have biases in cloud and radiation. The qualitative conclusion is unlikely to depend on these biases because it rests on the relative timing of freeze-up and break-up rather than on the absolute magnitude of the forcing, but the precise coefficients should be treated as estimates rather than as constants.

Fourth, the 2026 season is based on near-real-time passive-microwave data and may be revised. Fifth, the domain excludes Foxe Basin and Hudson Strait, where the ice regime differs, so the results apply to Hudson Bay and James Bay only.

4.5 *Future directions*

Three extensions follow naturally. The first is to repeat the analysis with satellite altimetry thickness, which would test the mechanism directly rather than by inference. The second is to apply the same seasonal-memory framework to other seasonally ice-covered seas, including the Baltic, the Sea of Okhotsk and the Bering Sea, to establish whether the coupling is a general property of seasonal ice or a feature of Hudson Bay's particular geometry. The third is to evaluate climate models on the relationship itself: a model that reproduces the trends but not the coupling is not reproducing the physics, and the memory coefficient provides a demanding and inexpensive diagnostic.

5. Conclusion

Hudson Bay's ice-free season lengthened by 6.8 days per decade between 1990 and 2026, from about 156 days in the early 1990s to about 186 days in the 2020s. The autumn end of the season moved more, and moved more reliably, than the spring end. The spring end nevertheless advanced, and it did so without any

detectable spring warming. The explanation is seasonal memory: a bay that freezes later in autumn breaks up earlier the following spring, by about half a day for every day of delay, independently of spring temperature. The relationship survives first-differencing, instrumental-variable estimation and double machine learning; it is present in 89% of grid cells; it has strengthened as the ice has thinned; and it accounts for roughly 70% of the observed spring advance.

The broader lesson is that the two ends of a seasonal ice cycle are not independent responses to the weather of their own season. They are linked by the ice itself, which integrates the autumn and carries it into the spring. Understanding that link improves seasonal prediction, sharpens attribution of observed change, and provides a diagnostic that climate models must pass if they are to be trusted in the region.

References

Anderson, D. L. (1961). Growth rate of sea ice. *Journal of Glaciology*, 3(30), 1170–1172.

Blanchard-Wrigglesworth, E., Bitz, C. M., & Holland, M. M. (2011). Influence of initial conditions and climate forcing on predicting Arctic sea ice. *Geophysical Research Letters*, 38(18), L18503. https://doi.org/10.1029/2011GL048807

Breiman, L. (2001). Random forests. *Machine Learning*, 45(1), 5–32. https://doi.org/10.1023/A:1010933404324

Chernozhukov, V., Chetverikov, D., Demirer, M., Duflo, E., Hansen, C., Newey, W., & Robins, J. (2018). Double/debiased machine learning for treatment and structural parameters. *The Econometrics Journal*, 21(1), C1–C68. https://doi.org/10.1111/ectj.12097

Day, J. J., Tietsche, S., & Hawkins, E. (2014). Pan-Arctic and regional sea ice predictability: Initialization month dependence. *Journal of Climate*, 27(12), 4371–4390. https://doi.org/10.1175/JCLI-D-13-00614.1

Derocher, A. E., Lunn, N. J., & Stirling, I. (2004). Polar bears in a warming climate. *Integrative and Comparative Biology*, 44(2), 163–176. https://doi.org/10.1093/icb/44.2.163

Fetterer, F., Knowles, K., Meier, W. N., Savoie, M., & Windnagel, A. K. (2017). *Sea Ice Index* (Version 4) [Data set]. National Snow and Ice Data Center. https://nsidc.org/data/g02135

Friedman, J. H. (2001). Greedy function approximation: A gradient boosting machine. *The Annals of Statistics*, 29(5), 1189–1232. https://doi.org/10.1214/aos/1013203451

Gagnon, A. S., & Gough, W. A. (2005). Trends in the dates of ice freeze-up and breakup over Hudson Bay, Canada. *Arctic*, 58(4), 370–382.

Gelaro, R., McCarty, W., Suárez, M. J., Todling, R., Molod, A., Takacs, L., Randles, C. A., Darmenov, A., Bosilovich, M. G., Reichle, R., Wargan, K., Coy, L., Cullather, R., Draper, C., Akella, S., Buchard, V., Conaty, A., da Silva, A. M., Gu, W., … Zhao, B. (2017). The Modern-Era Retrospective Analysis for Research and Applications, Version 2 (MERRA-2). *Journal of Climate*, 30(14), 5419–5454. https://doi.org/10.1175/JCLI-D-16-0758.1

Hochheim, K. P., & Barber, D. G. (2010). Atmospheric forcing of sea ice in Hudson Bay during the fall period, 1980–2005. *Journal of Geophysical Research: Oceans*, 115(C5), C05009. https://doi.org/10.1029/2009JC005334

Kendall, M. G. (1975). *Rank correlation methods* (4th ed.). Charles Griffin.

Lenssen, N. J. L., Schmidt, G. A., Hansen, J. E., Menne, M. J., Persin, A., Ruedy, R., & Zyss, D. (2019). Improvements in the GISTEMP uncertainty model. *Journal of Geophysical Research: Atmospheres*, 124(12), 6307–6326. https://doi.org/10.1029/2018JD029522

Lundberg, S. M., & Lee, S.-I. (2017). A unified approach to interpreting model predictions. In *Advances in Neural Information Processing Systems 30* (pp. 4765–4774). Curran Associates.

Mann, H. B. (1945). Nonparametric tests against trend. *Econometrica*, 13(3), 245–259. https://doi.org/10.2307/1907187

Markus, T., Stroeve, J. C., & Miller, J. (2009). Recent changes in Arctic sea ice melt onset, freezeup, and melt season length. *Journal of Geophysical Research: Oceans*, 114(C12), C12024. https://doi.org/10.1029/2009JC005436

Sen, P. K. (1968). Estimates of the regression coefficient based on Kendall's tau. *Journal of the American Statistical Association*, 63(324), 1379–1389. https://doi.org/10.1080/01621459.1968.10480934

Serreze, M. C., & Barry, R. G. (2011). Processes and impacts of Arctic amplification: A research synthesis. *Global and Planetary Change*, 77(1–2), 85–96. https://doi.org/10.1016/j.gloplacha.2011.03.004

Stroeve, J., Holland, M. M., Meier, W., Scambos, T., & Serreze, M. (2007). Arctic sea ice decline: Faster than forecast. *Geophysical Research Letters*, 34(9), L09501. https://doi.org/10.1029/2007GL029703

Stroeve, J. C., Markus, T., Boisvert, L., Miller, J., & Barrett, A. (2014). Changes in Arctic melt season and implications for sea ice loss. *Geophysical Research Letters*, 41(4), 1216–1225. https://doi.org/10.1002/2013GL058951

Appendix A. Data, code and derived quantities

All source data are publicly available. Sea-ice concentration: NASA National Snow and Ice Data Center, Sea Ice Index G02135 version 4.0, https://nsidc.org/data/g02135. Atmospheric fields: NASA POWER, https://power.larc.nasa.gov. Temperature anomalies: NASA GISTEMP v4, https://data.giss.nasa.gov/gistemp/. Imagery: NASA Worldview, https://worldview.earthdata.nasa.gov.

The processing mechanism is organized in a five-step procedure: retrieval of the daily concentration windows and the atmospheric grid; construction of the ice-season panel; estimation of trends and the seasonal-memory model; spatial estimation; and the machine-learning benchmark. The derived annual series (37 rows) and the cell-level coefficients (1,428 rows) are small enough to include as supplementary tables and are reproduced in the accompanying repository together with the code.

Reproducing the main results requires the daily concentration fields (approximately 250 MB compressed) and the atmospheric grid (approximately 60 MB). Both are cached by the retrieval scripts and regenerated deterministically from the public archives.

AI Use Statement. The author used an AI LLM model (Claude Fable 5.1 by Anthropic) to support this work for minor revisions only. The author used Claude only for small-scale language rendering, limited to grammar and word choice for fluent expression; terminology was excluded from this assistance. All data are from public archives and all computations are reproducible from the accompanying code. The author takes full responsibility for the originality, accuracy and interpretation of the work.

Supplementary Files

This is a list of supplementary files associated with this preprint. Click to download.

- SupplementaryCodeandData.zip